PV Cell Angle Optimization for Energy Generation-Consumption Matching in a Solar Powered Cellular Network

Doris Benda, *Student Member, IEEE*, Sumei Sun, *Fellow, IEEE*, Xiaoli Chu, *Senior Member, IEEE*, Tony Q. S. Quek, *Fellow, IEEE*, and Alastair Buckley

***Abstract*—An inherent problem of solar-energy-powered-small-cell base stations (SBSs) is that the energy generation of the photovoltaic (PV) cell does not match the energy consumption of the SBS in time. In this paper, we propose optimizing the PV cell orientation angle to achieve a good match between the energy generation and consumption profiles on a daily time scale. The optimization is formulated as an integer linear programming problem. We also derive an expression for the correlation between the energy generation and consumption profiles to evaluate their general interaction independent of the exact PV cell or SBS deployment setup. The numerical evaluation of the proposed angle optimization in a business area in London in summer/winter shows that the optimal PV cell orientation in summer contradicts the conventional assumption of south facing being optimal in the northern hemisphere. Instead, a southwest orientation should be chosen in summer due to its ability to shift the energy generation peak toward the energy consumption peak in the afternoon at an SBS in central London. This is in accordance with the prediction given by our derived correlation between the solar energy generation and consumption profiles.**

***Index Terms*—Green cellular network, PV cells, orientation angle, inclination angle, and downlink.**

I. Introduction

A. Background

THE INFORMATION and communications technology (ICT) accounts for 3% of the global electricity costs with an annual increase rate of 15-20% [2]. Base stations are responsible for more than half of the energy costs in the cellular network infrastructure [3], indicating a huge demand to take advantage of renewable energy generation. Experts estimated that energy harvesting technology can reduce 20% of the CO_2 emissions in the ICT industry [4].

The next generation cellular network requires a massive expansion of the small-cell base station (SBS) deployment [5]. In contrast to the increased energy consumption for operating large numbers of SBSs, many countries have set green taxation and incentive schemes to achieve ambitious CO_2 emission reduction targets, making renewable energy harvesting technologies attractive for cellular network operators. PV-cell-powered-SBSs have been considered for future cellular networks due to their small physical footprint in dense built environments, technology maturity, low maintenance cost and production cost reduction in recent years [4].

Main grid energy is always on demand whereas renewable energy faces the problem of spatial [6] and temporal variations [4]. These variations have to be managed properly and mitigation strategies such as combining wind and solar energy [4] have to be exploited to make efficient use of renewable energies. To the best of our knowledge, there has not been any reported study considering photovoltaic (PV) cell orientation angle optimization to mitigate the temporal variation of solar energy in a cellular network context. In addition, we could not find a study about a cellular network with a mixture of different orientated and/or inclined PV cells, which represents a more realistic cellular network.

B. Motivation - Energy Generation Profiles of PV Cells

The energy generation profile of a PV cell depends on the installed orientation θ and inclination γ angle. The inclination angle of a PV cell is defined as the angle between the horizontal plane and the PV cell panel. The orientation angle of a PV cell is defined as the angle between the southern direction and the projection of the line that points perpendicular out of the PV panel in the horizontal plane (see Fig. 1). Orientating the PV cell to the east (west) is indicated by a negative (positive) algebraic sign added to the orientation angle. For example, a SBS is depicted in Fig. 1 with $\theta = -45°$ and $\gamma = 38°$.

PV cells can be classified into fixed, sun tracking and adjustable PV cells (see Fig. 2). A fixed PV cell (see Fig. 2(a))

Manuscript received August 4, 2017; revised October 17, 2017; accepted November 2, 2017. Date of publication November 13, 2017; date of current version March 16, 2018. This work was supported in part by the A*STAR-Sheffield Research Attachment Programme and in part by the European Union's Horizon 2020 Research and Innovation Programme under Grant 645705. This work was partially presented at the IEEE International Conference on Communications, Paris, France, May 2017 [1]. The associate editor coordinating the review of this paper and approving it for publication was E. Ayanoglu. *(Corresponding author: Doris Benda.)*

D. Benda is with the Department of Electronic and Electrical Engineering, University of Sheffield, Sheffield S1 4ET, U.K., and also with the Communications and Networks Cluster, Institute for Infocomm Research, Singapore 138632 (e-mail: dcbenda1@sheffield.ac.uk).

S. Sun is with the Communications and Networks Cluster, Institute for Infocomm Research, Singapore 138632 (e-mail: sunsm@i2r.a-star.edu.sg).

X. Chu is with the Department of Electronic and Electrical Engineering, University of Sheffield, Sheffield S1 4ET, U.K. (e-mail: x.chu@sheffield.ac.uk).

T. Q. S. Quek is with the Information Systems Technology and Design Pillar, Singapore University of Technology and Design, Singapore 487372 (e-mail: tonyquek@sutd.edu.sg).

A. Buckley is with the Department of Physics and Astronomy, University of Sheffield, Sheffield S3 7RH, U.K. (e-mail: alastair.buckley@sheffield.ac.uk).

Digital Object Identifier 10.1109/TGCN.2017.2772910

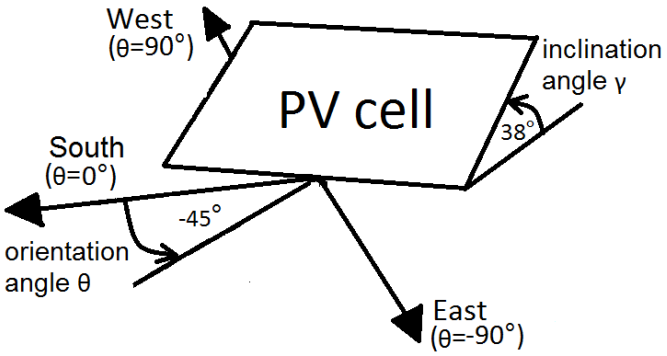

Fig. 1. Definition of the orientation angle θ and inclination angle γ of a PV cell.

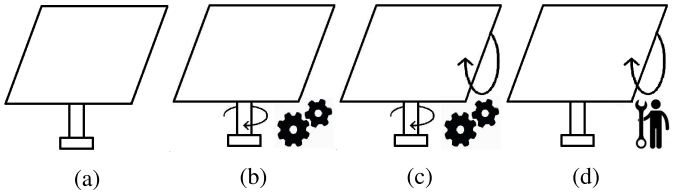

Fig. 2. Depiction of a fixed PV cell (a), single-axis tracking PV cell (b), two-axis tracking PV cell (c) and adjustable PV cell (d).

has fixed orientation and inclination angles which cannot be changed anymore after the initial installation. A single-axis tracking PV cell (see Fig. 2(b)) can mechanically track the sun throughout the day via adjusting the orientation angle. The single-axis tracking PV cell improves herein its daily energy yield compared to a fixed PV cell. A two-axis tracking PV cell (see Fig. 2(c)) can mechanically track the sun throughout the day and the season (e.g., winter and summer) via adjusting both the orientation and inclination angles. The two-axis tracking PV cell improves herein its yearly energy yield compared to a single-axis tracking PV cell. An adjustable PV cell (see Fig. 2(d)) requires an engineer to visit the site on a seasonable basis to adjust the angles manually.

Despite the potentially higher energy yield of sun tracking PV cells than fixed and adjustable PV cells, they are currently not widely deployed. The reasons are mainly the additional parts needed (e.g., axis motor), the higher maintenance (e.g., mechanical parts like the axis and the motor break more often than static parts), and the energy needed to operate the axis motor, which can be higher than the additional energy generated due to the sun tracking for some locations [7]. As a result, we do not consider sun tracking PV cells for deployment at a base station.

An engineer has to visit the adjustable PV cell on a seasonal basis to adjust the angles. Frequent/infrequent adjustments of the angles will result in higher/lower operational expenditure in combination with a higher/lower energy yield of the PV cell. In this paper, we will consider an adjustable PV cell which only needs to be visited twice a year (in spring and autumn equinox) to minimize the operational expenditure. Nonetheless, our derived optimization process can equivalently be used to optimize the angles more frequently or to optimize the fixed angles of a fixed PV cell. Fixed PV cells can be seen as a special case of an adjustable PV cell that does not require additional visits of engineers after its initial installation.

TABLE I
DEFAULT OPTIMAL ORIENTATION AND INCLINATION ANGLE FOR DIFFERENT LOCATIONS [8]

Location	Default optimal orientation angle θ	Default optimal inclination angle γ
Northern hemisphere	0°	similar to the location's latitude
Southern hemisphere	180°	similar to the location's latitude
Equator	any angle between -180 and 180°	0°

There exist a default optimal PV cell orientation and inclination angle for a given geographical location of a SBS, which provides the highest average solar energy yield per day [8]. TABLE I gives an overview of the default optimal orientation and inclination angles for a PV cell located at the equator, in the northern hemisphere and in the southern hemisphere. However, the default energy generation profile may differ from the energy consumption demand profile.

PV cells with suboptimal orientation and/or inclination angles generate less solar energy in total. Adjusting the orientation angle has been shown to shift the daily solar energy generation profile in the time domain (see Fig. 3). Changing the inclination angle, on the other hand, shifts the solar energy generation profile on a yearly time scale. Locations directly at the equator have a default optimal inclination angle of 0°. Therefore, all orientation angles have the same daily solar energy generation profile at the equator.

C. Motivation - Energy Consumption Profiles of SBSs

The energy consumption profile at a SBS is linked to the traffic load profile of the deployment area. For example, residential and business areas have anti-correlated traffic load profiles, because during the time of the day when people are usually at work/at home, the traffic load in the business/residential area rises while the traffic load in the residential/business area declines [9].

D. Contributions

In this paper, we optimize the PV cell orientation angle to achieve a good match between the energy generation and consumption profiles at a PV-cell-powered-SBS on a daily time scale.

The contributions of the paper can be summarized as follows:

- We present an analytical framework incorporating the effects of different inclination and orientation angles at a PV-cell-powered-SBS.
- We develop an integer linear programming problem to optimize the orientation angle for any given PV cell and SBS deployment setup.
- We derive a mathematical expression for the correlation factor between the energy generation and consumption profiles to evaluate the general interaction between both profiles independent of the exact PV cell and SBS deployment setup.

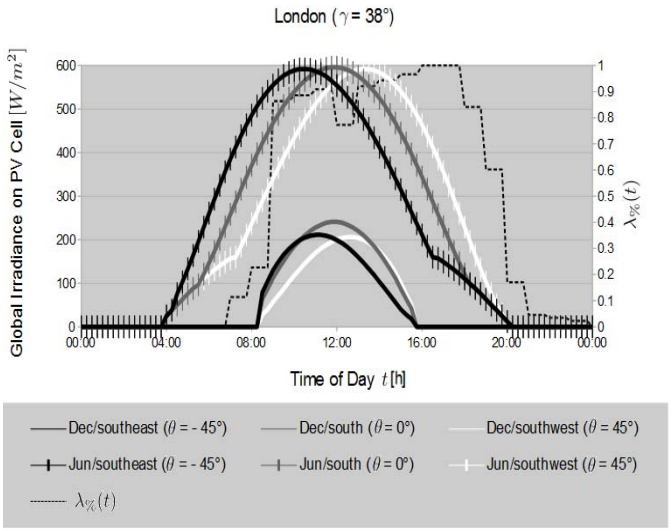

Fig. 3. Daily global irradiance profiles of differently orientated PV cells in London in December (no marker, solid line data series, left y-axis) and in June (vertical bar marker, solid line data series, left y-axis). PV cell orientation to the southeast, south and southwest are colored black, gray and white, respectively. The default optimal orientation (inclination) angle is 0° (38°) for London. Daily user density $\lambda_{\%}(t)$ profile in a business area (dashed line data series, right y-axis). The user density is given as a percentile of the maximum user density per hour. Data source: [9], [10].

- We evaluate the effects of different PV cell orientation angles on the solar energy utilization of the SBS in different seasons based on a case study in London.

The rest of the paper is organized as follows. Sections II-A to II-C present a general energy generation, storage and consumption model of a PV-cell-powered-SBS, which includes the effects of PV cell orientation and inclination. Section II-D derives the mathematical expression for the correlation factor between the energy generation and consumption profiles. Section III outlines the integer linear programming problem to optimize the energy performance of the SBS throughout the day. Section IV presents and discusses the numerical results of the integer linear programming problem based on a case study in a London business area. Section V evaluates the general interaction between the energy generation and consumption profiles on the basis of the correlation factor. Finally, the paper is concluded in Section VI.

Notations: All matrices are denoted by bold capital letters, all vectors are denoted by bold lowercase letters, and an asterisk is added to the letter if it is an optimized matrix, vector or value.

II. System Model

A. SBS Model

The SBS has a coverage area radius of r and is completely powered by a PV cell with no main grid energy supply. The SBS becomes inactive if no user equipment (UE) is in its coverage area or when the SBS runs out of energy. If the SBS cannot serve its UEs, we assume that the UEs are offloaded to a different tier in the heterogeneous cellular network, e.g., a main grid connected macro base station. It is not in the scope of this paper to analyze the performance of this macro base station tier. The setups of the SBS and PV panel will be fixed except that we alter the orientation angle to achieve a daily shift in the energy generation profile.

B. Solar Energy Generation Model

There are four astronomical events (equinox in March and September, solstice in June and December), which significantly affect the solar energy arrival in most geographical areas. Therefore, the solar energy harvesting model has to take these annual differences into account and be evaluated throughout the year to represent the different seasons accordingly.

A day is divided into T time steps. Denote t as the index of a time step, $t \in \{1, \ldots, T\}$. The energy harvesting profile of the SBS correlates with the solar irradiance. The generated solar energy $g_\theta^{(t)}$ at the SBS in the t^{th} time step is given by

$$g_\theta^{(t)} = G_\theta^{(t)} \cdot \eta \cdot A \cdot \bar{t} \tag{1}$$

where $G_\theta^{(t)}[\mathrm{W/m^2}]$ is the global irradiance value on the PV cell deployed with orientation angle θ in the t^{th} time step [10], η is the PV cell energy conversion efficiency coefficient, $A[\mathrm{m^2}]$ is the surface area of the PV cell, and $\bar{t}$[s] is the length of one time step.

The global irradiance value $G_\theta^{(t)}$ is derived from the data base [10], which provides data for any combination of orientation angle, inclination angle, month and location in Europe and Asia, with a 15-minute time resolution. The harvested solar energy in each time step can either be immediately consumed by the SBS or stored in a battery of capacity $b_{\max}$.

C. Solar Energy Consumption Model and Traffic Load Model

The energy consumption of a SBS can be divided in a load-independent part and a load-dependent part. The load-independent energy consumption is constant throughout all time steps and is donated as c_{fix}. It includes the energy consumption of the baseline operations, such as transmitting signal beacons and circuit cooling operations. The load-dependent energy consumption per time step increases with the number of UEs connected to the SBS due to the increased traffic load. Accordingly, the total energy consumption $c^{(t)}$ of the SBS in the t^{th} time step is given by

$$c^{(t)} = c_{\mathrm{fix}} + c_{\mathrm{user}} \cdot l^{(t)} \tag{2}$$

where c_{fix} and $c_{\mathrm{user}} \cdot l^{(t)}$ denote the load-independent and load-dependent energy consumption, respectively, whereas c_{user} is the average energy consumed by the SBS for serving one UE during a time step, and $l^{(t)}$ is the total number of UEs located in the coverage area of the SBS in the t^{th} time step.

The total number of UEs located in the coverage area of the SBS in the t^{th} time step is calculated based on the downlink traffic distribution over time in a business district (see Fig. 3) as follows

$$l^{(t)} = \lfloor \lambda_{\%}(\lfloor t \rfloor_h) \cdot u_{\max} \rceil \quad \forall t \in \{1, \ldots, T\} \tag{3}$$

where the time step t is rounded down to the nearest full hour, $\lambda_{\%}(\lfloor t \rfloor_h)$ is the user density at $\lfloor t \rfloor_h$ according to Fig. 3, and

$u_{\max}$ is the maximum number of UEs in the coverage area of the SBS. $l^{(t)}$ is rounded to the nearest integer value indicated by the rounding-brackets "$\lfloor\,\rceil$".

D. Correlation Factor

To facilitate the analysis of the energy generation and consumption matching, we give a mathematical expression for the correlation factor $(g \star c)[\theta]$ between an energy generation profile g with orientation angle θ and a consumption profile c. In general, a correlation factor is defined in the range of [0, 1], whereas a value close to 0 (1) represents a strong anti-correlation (correlation) between the two profiles. We normalize both profiles on the basis of the consumption profile and denote the normalized energy generation/consumption at time step t as ${}^N g_\theta^{(t)}$/ ${}^N c^{(t)}$. As a result, the area under the normalized consumption profile in Figs. 5(a)-5(c) is 1.

$$ {}^N g_\theta^{(t)} = \frac{g_\theta^{(t)}}{\sum_{t=1}^{T} c^{(t)}} \tag{4} $$

$$ {}^N c^{(t)} = \frac{c^{(t)}}{\sum_{t=1}^{T} c^{(t)}} \tag{5} $$

We use the following definition of the correlation factor which is bounded by 1 due to the normalization. The justification for using this definition is given in Appendix A.

$$ 0 \le (g \star c)[\theta] \stackrel{def}{=} \sum_{t=1}^{T} \min\left\{ {}^N g_\theta^{(t)}, {}^N c^{(t)} \right\} \le \sum_{t=1}^{T} {}^N c^{(t)} = 1 \tag{6} $$

The correlation factor $(g \star c)[\theta]$ can be graphically depicted as joint area under the two profiles (see black area in Figs. 5(a)-5(c)). Therefore, $(g \star c)[\theta]$ is a measure for the ability of the energy generation profile g to provide temporally enough energy for the consumption profile c. Using an oversized PV cell (large PV cell surface area) will result in a high $(g \star c)[\theta]$ value. But if the PV cell settings are fixed and only the orientation angle alters, a higher $(g \star c)[\theta]$ value represents a better correlation between the energy generation and consumption profiles. The orientation angle which achieves the highest correlation factor for a specific PV cell setting is denoted as $\theta^*_{(g \star c)}$ and refereed to as optimized orientation on the basis of the correlation factor.

$$ \theta^*_{(g \star c)} = \arg \max_{\theta \in \{-90°, -85°, \ldots, 85°, 90°\}} (g \star c)[\theta] \tag{7} $$

The gap Δ between the optimized correlation factor $(g \star c)[\theta^*_{(g \star c)}]$ and the default correlation factor with PV cell orientation to the south $(g \star c)[0]$ is defined as follows

$$ \Delta = (g \star c)\left[\theta^*_{(g \star c)}\right] - (g \star c)[0]. \tag{8} $$

III. PV Cell Orientation Angle Optimization With an Integer Linear Program

The aim of the optimization is to maximize the total load that can be supported by the SBS during T time steps. It is achieved by optimizing the on = 1/off = 0 statuses of the SBS, which are described as Boolean variables $o_\theta^{(t)} \in \{0, 1\}$ for $t \in \{1, \ldots, T\}$. The SBS serves every UE in its coverage area with one load block per time step when it is on. That means the SBS needs c_{user} Joules of energy to serve one load block. The SBS does not serve any UE when it is off. Therefore, the total load blocks served per day R_θ can be calculated as

$$ R_\theta = \sum_{t=1}^{T} o_\theta^{(t)} l^{(t)}. \tag{9} $$

The SBS is equipped with a battery of capacity $b_{\max}$. The battery levels in two successive time steps are linked through

$$ b_\theta^{(t)} = b_\theta^{(t-1)} + g_\theta^{(t-1)} - w_\theta^{(t-1)} - c^{(t-1)} \cdot o_\theta^{(t-1)} \quad \forall t \in \{2, \ldots, T\} \tag{10} $$

where $b_\theta^{(t)}$ and $b_\theta^{(t-1)} (\in [0, b_{\max}])$ donate the battery levels of the SBS in the t^{th} and $(t-1)^{th}$ time step, respectively, $g_\theta^{(t-1)}$ is the amount of generated solar energy by the SBS in the $(t-1)^{th}$ time step, $c^{(t-1)}$ and $w_\theta^{(t-1)}$ denote the energy consumption and the wasted energy due to battery overflow at the SBS in the $(t-1)^{th}$ time step, respectively.

Let the vector $\boldsymbol{o_\theta} = \{o_\theta^{(1)}, o_\theta^{(2)}, \ldots, o_\theta^{(T)}\}$ denote the on/off statuses of the SBS over T time steps. The optimization problem is formulated as follows

$$ \boldsymbol{o^*_\theta} = \arg \max_{\boldsymbol{o_\theta}} R_\theta. \tag{11} $$

subject to

$$ \mathbf{0}^\intercal \le \boldsymbol{b_\theta^{(0)}}^\intercal + \mathbf{M}^1 \cdot \left(\boldsymbol{g_\theta}^\intercal - \boldsymbol{w_\theta}^\intercal\right) - \mathbf{M}^c \cdot \boldsymbol{o_\theta}^\intercal \le \boldsymbol{b_{\max}}^\intercal \tag{12} $$

$$ g_\theta^{(t)}, w_\theta^{(t)} \ge 0 \quad \forall t \in \{1, \ldots, T\} \tag{13} $$

$$ l^{(t)} \in \mathbb{N}_0 \quad \forall t \in \{1, \ldots, T\} \tag{14} $$

$$ o_\theta^{(t)} \in \{0, 1\} \quad \forall t \in \{1, \ldots, T\} \tag{15} $$

$$ 0 \le b_\theta^{(0)} \le b_{\max} \tag{16} $$

where the vectors are of size T and are defined as

$$ \boldsymbol{g_\theta} = \left\{g_\theta^{(1)}, g_\theta^{(2)}, \ldots, g_\theta^{(T)}\right\}, \quad \mathbf{0} = \left\{\underbrace{0, \ldots, 0}_{T}\right\}, $$

$$ \boldsymbol{o_\theta} = \left\{o_\theta^{(1)}, o_\theta^{(2)}, \ldots, o_\theta^{(T)}\right\}, \quad \boldsymbol{b_{\max}} = \left\{\underbrace{b_{\max}, \ldots, b_{\max}}_{T}\right\}, $$

$$ \boldsymbol{w_\theta} = \left\{w_\theta^{(1)}, w_\theta^{(2)}, \ldots, w_\theta^{(T)}\right\}, \text{ and } \boldsymbol{b_\theta^{(0)}} = \left\{\underbrace{b_\theta^{(0)}, \ldots, b_\theta^{(0)}}_{T}\right\} $$

and the two matrices $\mathbf{M}^1$ and $\mathbf{M}^c$ are of size TxT, with the element in the i^{th} row and the j^{th} column given by

$$ \mathbf{M}^1(i,j) = \begin{cases} 1 & \text{if } i \ge j \\ 0 & \text{otherwise} \end{cases} \tag{17} $$

$$ \mathbf{M}^c(i,j) = \begin{cases} c^{(j)} & \text{if } i \ge j \\ 0 & \text{otherwise} \end{cases} \tag{18} $$

Equation (12) keeps the battery level within the range of $[0, b_{\max}]$ in every time step. The $t^{th} (t \in \{1, \ldots, T\})$

TABLE II
INPUT PARAMETERS TO THE OPTIMIZATION PROBLEM (11)

Parameter	Value
θ	$\in \{-45°, 0°, 45°\}$
γ	38° [10]
Month	June and December
Latitude (London)	$51°30'26''$ North
Longitude (London)	$0°7'39''$ West
T	96
$\bar{t}$	$15\text{min} = 900\text{s}$
c_{fix}	34965J
c_{user}	80J
$b_{\max}$	86400J
$b_\theta^{(0)}$	0J
$u_{\max}$	$471 \frac{\text{UE}}{\text{r}^2\pi}$
A	1m^2
η	0.15
$g_\theta^{(t)}$	cf. (1)
$l^{(t)}$	cf. (3)

TABLE III
PERCENTAGE OF LOAD BLOCKS SERVED BY THE SBS DURING ONE DAY

	Percentage of load blocks served by the SBS
December (southeast)	17.40%
December (south)	20.60%
December (southwest)	17.60%
June (southeast)	65.76%
June (south)	74.84%
June (southwest)	80.34%

row in $\mathbf{M}^1$ and $\mathbf{M}^c$ describes time step t. The t^{th} row of Equation (12) is obtained by recursively substituting (10) into $0 \leq b_\theta^{(t)} \leq b_{\max}$ for t times. The values of $g_\theta^{(t)}$ and $l^{(t)}$ are input parameters to the optimization problem. As described in Sections II-B and II-C, the values of $g_\theta^{(t)}$ can be derived from the database [10], and the values of $l^{(t)}$ are based on Fig. 3. Network operators can more reliably determine the values of $g_\theta^{(t)}$ by contacting the local meteorological forecast service and the values of $l^{(t)}$ by using their historical records of the local traffic load distribution.

IV. NUMERICAL SOLUTION TO THE INTEGER LINEAR OPTIMIZATION

To evaluate the effects of different PV cell orientations on the performance of the SBS, we investigate three different orientation angles $\theta \in \{-45°$ (southeast), 0° (south), 45° (southwest)$\}$ with the integer linear programming problem. The default optimal inclination angle for London is fixed to 38° [10]. The optimization problem (11) is solved for the three orientation angles separately. TABLE II shows the input parameters of the optimization problem (11) assuming that the SBS deployment is in London in December and June. The justification for used battery capacity is given in Appendix B.

The optimization problem (11) is an integer linear programming problem and can be solved using the simplex algorithm and the branch & bound method, which are available as an integer linear optimization solver in mathematical software packages such as MATLAB.

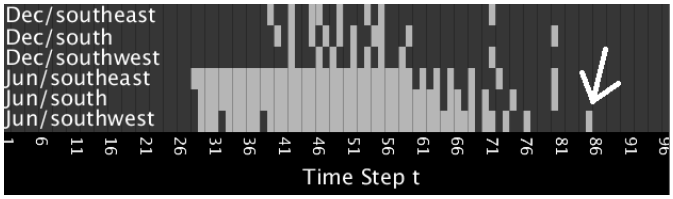

Fig. 4. On=light gray/off=dark gray status values of the simulated southeast, south and southwest orientated SBS in December and June.

A. Comparison of Different Orientations

The southwest/southeast orientated SBS is more likely to be on later/earlier in the day than the south orientated SBS in both months (see Fig. 4). This is caused by the solar energy profile output, which is shifted towards the afternoon/morning hours for the southwest/southeast orientated SBS compared to the southern SBS.

1) Comparison of Different Orientations in Winter: Southeast and southwest orientated PV cells can serve 17.40% and 17.60% of their load blocks, respectively, whereas the southern PV cell can serve with 20.60% the most load blocks from all three different orientations in winter (see TABLE III). This is caused by the fact that the southeast and southwest orientated PV cells generate less energy during this time of the year compared to the default south orientated one (see Fig. 3), therefore they can serve fewer load blocks. The performance of the southeast and southwest SBS is nearly the same in winter because they generate the same amount of energy during the day (see Fig. 3) and all this energy is used to serve load blocks. This is only the case because battery overflows occur very rarely in winter due to the significantly lower energy generation profile than the energy consumption profile in winter.

2) Comparison of Different Orientations in Summer: The situation is different during the summer month June, where the southwest orientated PV cell has the best performance and can serve 80.34% of its load blocks (see TABLE III). This is due to the shifted PV cell energy generation profile of the southwestern PV cell towards the afternoon hours, which is similar to the traffic load profile. This proves that the southwestern orientation has a positive effect by adjusting the energy generation profile of the SBS to the consumption profile, so that less green energy is wasted due to less battery overflow. The second best performance in summer is achieved by the southern PV cell with 74.84%, followed by the southeastern PV cell with 65.76% (see TABLE III). Despite the southeast PV cell generates the same total amount of energy throughout the day than the southwest PV cell (see Fig. 3), it wastes more energy than the southwest PV cell due to battery overflow in the morning hours when the energy consumption is low but the energy generation profile of the southeast PV cell is already high.

B. Comparison of Different Seasons

In general, all PV cells serve more load blocks during summer than winter due to their higher solar irradiance yield in

this month (see TABLE III). The misalignment of the southwestern and southeastern PV cell in summer has not such a negative effect on the total energy generation of these PV cells throughout the day than in winter (see Fig. 3) because the sun is higher up on the horizon in summer.

C. Additional Comments

It can be observed that for example the SBS (Jun/southwest) is suddenly on at time step 85 (see white arrow in Fig. 4), but there is not a lot of energy arriving at that time. This is due to the fact that the SBS has accumulated energy for many time steps so that there is sufficient energy available to serve load blocks for one time step.

V. Correlation Factor Comparison

We evaluate the correlation factor of the energy generation and consumption profiles defined in Section II-D. Data from London in summer (June) is used for the analysis, but the model considered is generic. The following three cases are investigated separately.

- Case 1: Energy generation significantly lesser than energy consumption ($G << C$) as depicted in Fig. 5(a).
- Case 2: Energy generation similar to energy consumption ($G = C$) as depicted in Fig. 5(b).
- Case 3: Energy generation significantly greater than energy consumption ($G >> C$) as depicted in Fig. 5(c).

Fig. 6 shows the correlation factor for different orientation angles for all three Cases 1-3. The circled marked data points are the optimal correlation factors for each data series. The orientation angles associated with these circle marked data points are the optimal orientation angles $\theta^*_{(g\star c)}$ for each PV cell surface area setting $A = 0.5\text{m}^2$, 1.2m^2 or 2m^2.

Each data series is carried out with the same PV cell setting (same PV cell surface area). Therefore, the change in the correlation factor within one data series is only caused by a change in the correlation between the energy generation and consumption profile for the different orientation angles.

The shape of the data series curves are different for each case. The energy generation profile is under the energy consumption profile in Case 1. Therefore, the greatest correlation factor is achieved in this data series by the energy generation profile with the greatest area under its profile which is close to the south orientated energy generation profile in London.

Because the energy generation and consumption profiles have similar amplitudes in Case 2, the highest correlation factor is achieved by an orientation angle which shifts the energy generation peak towards the energy consumption peak in this data series. The optimal orientation angle is 60° for $A = 1.2\text{m}^2$.

The energy generation is significantly larger than the energy consumption in Case 3. As a result, shifting the energy generation completely to the afternoon ($\theta^*_{(g\star c)} = 90°$) achieves the highest correlation factor because the energy consumption at the transition between both profiles is higher in the afternoon hours (see right gray circle in Fig. 5(c)) than in the morning hours (see left gray circle in Fig. 5(c)).

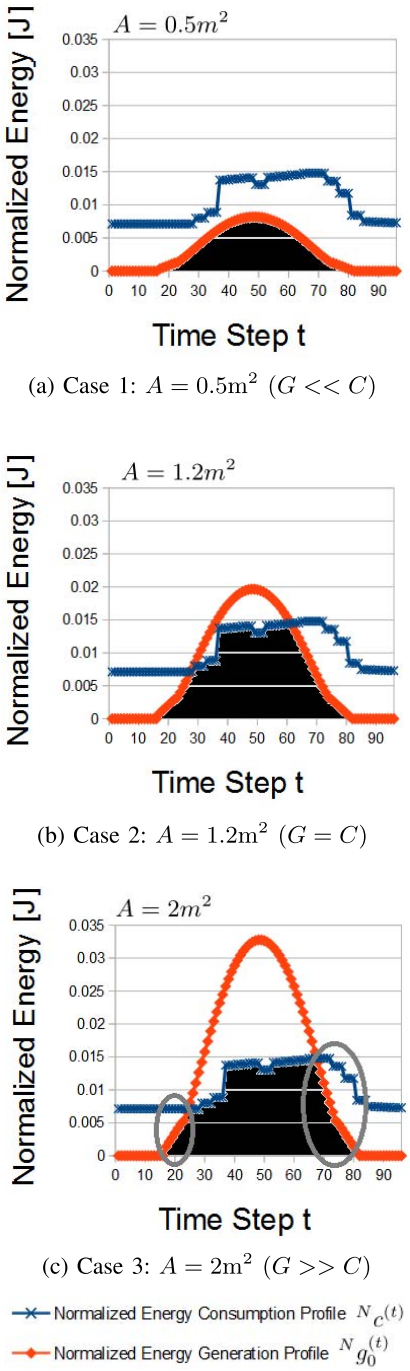

Fig. 5. Normalized energy generation and consumption profiles for London in summer (Case 1-3). The correlation factor is depicted as black area. The PV cell surface areas $A = 0.5\text{m}^2$, $A = 1.2\text{m}^2$ and $A = 2\text{m}^2$ are used for Case 1, 2 and 3, respectively. All other input parameters are given in TABLE II.

An increase in the PV cell surface area A results in an increase of the correlation factor as it can be seen in Fig. 6 where the Case 3 data series is above Case 2 data series and Case 2 data series is above Case 1 data series. Nonetheless, the increase slows down because the correlation factor is bounded by 1. That means even if A goes to infinity the correlation factor will be bounded by 1. That is the reason why the increase between the Case 1/2 data series is greater than between the Case 2/3 data series. It can be explained by the fact that

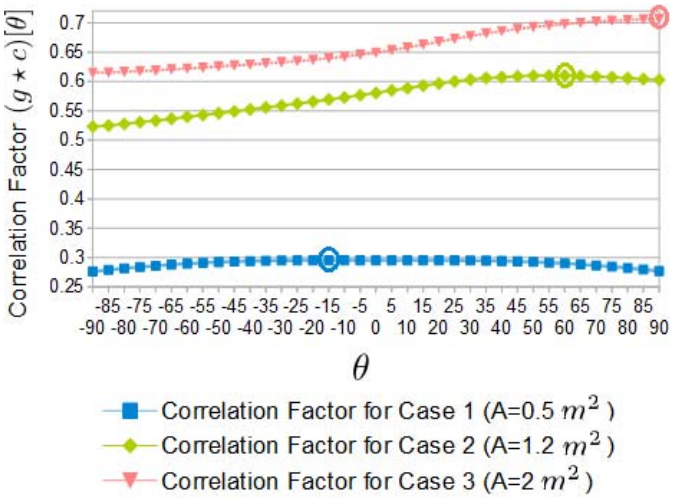

Fig. 6. Correlation factor $(g \star c)[\theta]$ for different orientation angles θ for all three Cases 1-3. The data points associated with the optimal correlation factor $(g \star c)[\theta^*_{(g \star c)}]$ and optimal orientation angle $\theta^*_{(g \star c)}$ are marked with a circle for each data series. Input parameters: London (June), $A = 0.5\text{m}^2$, 1.2m^2 or 2m^2 and remaining parameters from TABLE II.

$(g \star c)[\theta]$ sums up the expression "$\min\{{}^N g_\theta^{(t)}, {}^N c^{(t)}\}$" over all time steps. The expression "$\min\{{}^N g_\theta^{(t)}, {}^N c^{(t)}\}$" increases for all time steps between the Case 1/2 data series whereas it increases only at the transition time steps (see gray circles in Fig. 5(c)) between the Case 2/3 data series.

Fig. 6 explains the results which we observed at the numerical results evaluation in Section IV. The conditions in London during winter are similar to Case 1 with $G << C$. The analytical evaluation in this Section confirms that $\theta^*_{(g \star c)}$ is around the south orientation for Case 1 (see circled marked data point around the square marker in Fig. 6). The numerical results evaluation in Section IV proves the same by favoring the south orientation over the southeast and southwest orientation. The conditions in London during summer are similar to Case 2 with $G = C$. The analytical evaluation in this Section confirms that $\theta^*_{(g \star c)}$ is shifted towards the west orientation for Case 2 (see circled marked data point around the diamond marker in Fig. 6). The numerical results evaluation in Section IV proves the same by favoring the southwest orientation over the southeast and south orientation.

Fig. 7 shows the correlation factor for the default south orientation $(g \star c)[0]$ and the correlation factor for the optimized orientation $(g \star c)[\theta^*_{(g \star c)}]$ for different PV cell surface sizes A on the left y-axis. In addition, it depicts the optimized orientation angle $\theta^*_{(g \star c)}$ on the right y-axis for different PV cell surface sizes A.

It can be seen that the optimized orientation angle is close to the south orientation ($\theta^*_{(g \star c)} = 0°$) in the Case 1 sector and therefore both correlation factor curves are above each other $(g \star c)[0] = (g \star c)[\theta^*_{(g \star c)}]$. In addition, the correlation factor curves rise linear in the Case 1 sector. Doubling the PV cell surface area, doubles the area under the energy generation profile which doubles the correlation factor in the Case 1 sector because the energy generation profile is completely under the energy consumption profile in the Case 1 sector.

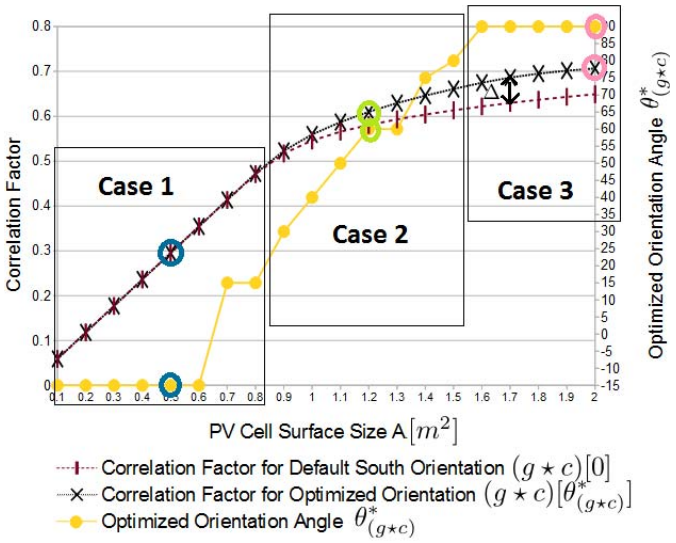

Fig. 7. The left y-axis shows the correlation factor for the default south orientation and the correlation factor for the optimized orientation for different PV cell surface sizes. The right y-axis shows the optimized orientation angle for different PV cell surface sizes. The circled marked data point around the square, diamond and triangle marker in Fig. 6 correspond to the two circled marked data points in the Case 1, 2 and 3 sector in Fig. 7, respectively. The correlation factor gap Δ and the Case 1, 2 and 3 sectors are depicted graphically. Input parameters: London (June) and remaining parameters from TABLE II.

TABLE IV
COST AND GAIN COMPARISON FOR THE DIFFERENT CASES

	Cost		Gain
	PV cell size cost	PV cell angle optimization cost	Correlation factor gap Δ (Energy saving due to optimized correlation)
Case 1 $G << C$	low	low ($\theta^*_{(g \star c)} = 0°$)	low
Case 2 $G = C$	medium	high ($\theta^*_{(g \star c)}$ has to be calculated)	medium
Case 3 $G >> C$	high	low ($\theta^*_{(g \star c)} = 90°$)	high

The Case 2 sector is the transition phase. The optimized orientation angle $\theta^*_{(g \star c)}$ moves from the south orientation to the west orientation with rising PV cell surface size. As a result, the gap Δ between $(g \star c)[\theta^*_{(g \star c)}]$ and $(g \star c)[0]$ increases accordingly.

The optimized orientation angle $\theta^*_{(g \star c)}$ has settled down to the west orientation in the Case 3 sector. The gap between $(g \star c)[0]$ and $(g \star c)[\theta^*_{(g \star c)}]$ is not changing significantly anymore with rising PV cell surface size. The rise of both correlation factors slow down because they are bounded by 1.

The circled marked data points associated with the optimal correlation factor $(g \star c)[\theta^*_{(g \star c)}]$ and optimal orientation angle $\theta^*_{(g \star c)}$ for the three PV cell surface area settings from Fig. 6 can be found in Fig. 7 as well. The circled marked data point around the square, diamond and triangle marker in Fig. 6 correspond to the two circled marked data points in the Case 1, 2 and 3 sector in Fig. 7, respectively.

The three Cases 1-3 are summarized in TABLE IV. Boxes which are associated with low cost or high gain are highlighted in dark gray. The dark gray boxes are the desired boxes.

TABLE IV helps to identify the best deployment strategy (Case 1, 2 or 3) if the exact PV cell module cost, orientation optimization cost and main grid energy cost are known.

VI. Conclusion

We have investigated the effects of different orientated PV cells on the solar energy utilization of a SBS. Our numerical results show that southwest orientated PV cells ($\theta = 45°$) can serve more load blocks throughout the day than south or southeast ($\theta = -45°$) orientated ones in London in summer (business area). The southwest orientation of the PV cell shifts the energy generation peak towards the energy consumption peak of the SBS and therefore serves more load blocks. This result contradicts the conventional assumption that the southern orientation is the optimal orientation in the northern hemisphere. It is therefore important to take into account the exact energy generation profile and consumption profile of the SBS's deployment site to determine the optimal PV cell orientation. Our analytical evaluation of the correlation factor between the energy generation profile of the PV cell and the energy consumption profile of the SBS concluded the same results.

Appendix A
Justification for the Used Definition of the Correlation Factor

Normally the cross-correlation is used as correlation factor (see Eq. (19)).

$$\theta^*_{(g\star c)} \stackrel{def}{=} \sum_{t=1}^{T} g[t+\theta]c[t] \tag{19}$$

Eq. (19) would shift the energy generation profile g only θ steps in the time domain and not represent the decline of the amplitude in the energy generation profile when shifting the profile θ steps away from the default south orientation ($\theta = 0°$). We could include the amplitude change in the definition (see Eq. (20)).

$$\theta^*_{(g\star c)} \stackrel{def}{=} \sum_{t=1}^{T} g_\theta^{(t)} c^{(t)} \tag{20}$$

Eq. (20) can not be bounded by 1 even after normalization. If the PV cell surface size goes to infinity, the energy generation profile amplitude goes to infinity and as a result the correlation factor goes to infinity. As a result, we decided to define the correlation factor as given in Eq. (6), because it represents the amplitude change correctly and can be bounded by 1 after normalization.

Appendix B
Justification for the Used Battery Capacity

The derived results in this paper depend on the used battery capacity due to the fact that a greater battery capacity can store more energy over a longer period of time. Increasing the battery capacity improves the energy utilization of the SBS in a similar way to orientation angle optimization in terms of shifting the energy from a surplus time period to a deficit time period. The reader is referred to our paper [11], which investigates this dependency in more detail. In general, PV cell orientation angle optimization is more important for PV-cell-powered-SBSs with small battery capacities in relationship to their energy profiles.

From a practical point of view, we can achieve a good match of the profiles by either installing a small battery with orientation angle optimization or installing a large battery without orientation angle optimization. Nonetheless, batteries are expensive (25-250€, 220€ and 1500€ per kWh for the battery types Lead-Acid, NaS and Li-Ion, respectively [12]) and have a short lifetime (3–9 years [13]) compared to the warranty lifetimes of PV cells (PV cell manufacturers guarantee a 80% system performance warranty for around 20 years [14]). Therefore, battery replacements significantly contribute to the system lifetime cost [13]. Small batteries with orientation angle optimization are practically the more cost-effective option. This is why we have chosen low-capacity batteries in this paper and make use of orientation angle optimization for matching the energy generation and consumption profiles.

References

[1] D. Benda, X. Chu, S. Sun, T. Q. S. Quek, and A. Buckley, "PV cell angle optimisation for energy arrival-consumption matching in a solar energy harvesting cellular network," in *Proc. IEEE Int. Conf. Commun.*, Paris, France, May 2017, pp. 1–6.

[2] Y. Wu *et al.*, "Green transmission technologies for balancing the energy efficiency and spectrum efficiency trade-off," *IEEE Commun. Mag.*, vol. 52, no. 11, pp. 112–120, Nov. 2014.

[3] A. Kwasinski and A. Kwasinski, "Increasing sustainability and resiliency of cellular network infrastructure by harvesting renewable energy," *IEEE Commun. Mag.*, vol. 53, no. 4, pp. 110–116, Apr. 2015.

[4] Y. Mao, Y. Luo, J. Zhang, and K. B. Letaief, "Energy harvesting small cell networks: Feasibility, deployment, and operation," *IEEE Commun. Mag.*, vol. 53, no. 6, pp. 94–101, Jun. 2015.

[5] G. Piro *et al.*, "HetNets powered by renewable energy sources: Sustainable next-generation cellular networks," *IEEE Internet Comput.*, vol. 17, no. 1, pp. 32–39, Jan./Feb. 2013.

[6] K. Huang, M. Kountouris, and V. O. K. Li, "Renewable powered cellular networks: Energy field modeling and network coverage," *IEEE Trans. Wireless Commun.*, vol. 14, no. 8, pp. 4234–4247, Aug. 2015.

[7] R. Eke and A. Senturk, "Performance comparison of a double-axis sun tracking versus fixed PV system," *Solar Energy*, vol. 86, no. 9, pp. 2665–2672, 2012.

[8] A. Luque and S. Hegedus, *Handbook of Photovoltaic Science and Engineering*, 2nd ed. Chichester, U.K.: Wiley, 2011.

[9] CelPlan. (2014). *White Paper—Customer Experience Optimization in Wireless Networks*. [Online]. Available: http://www.celplan.com/resources/whitepapers/Customer%20Experience%20Optimization%20rev3.pdf

[10] European Commission. (2016). *Photovoltaic Geographical Information System (PVGIS)*. [Online]. Available: http://re.jrc.ec.europa.eu/pvgis/

[11] D. Benda, X. Chu, S. Sun, T. Q. S. Quek, and A. Buckley, "PV cell orientation angle optimization for a solar energy harvesting base station," in *Proc. IEEE Glob. Commun. Conf.*, Dec. 2017, pp. 1–6.

[12] V. Rudolf and K. D. Papastergiou, "Financial analysis of utility scale photovoltaic plants with battery energy storage," *Energy Policy*, vol. 63, pp. 139–146, Dec. 2013.

[13] A. F. Crossland, O. H. Anuta, and N. S. Wade, "A socio-technical approach to increasing the battery lifetime of off-grid photovoltaic systems applied to a case study in rwanda," *Renew. Energy*, vol. 83, pp. 30–40, Nov. 2015.

[14] M. A. S. Alshushan and I. M. Saleh, "Power degradation and performance evaluation of PV modules after 31 years of work," in *Proc. IEEE 39th Photovolt. Specialists Conf. (PVSC)*, Tampa, FL, USA, Jun. 2013, pp. 2977–2982.

Doris Benda (S'17) received the B.Sc. degree in mathematics from the University of Bonn, Germany, in 2014 and the M.Sc. degree from Liverpool John Moores University, U.K., in 2015. She is currently pursuing the Ph.D. degree in electrical engineering with the University of Sheffield, U.K. Since 2016, she has been with the Institute for Infocomm Research, Singapore. Her research interests span various areas in green communication and network optimization, especially the incorporation of renewable energy in the cellular network. She was a recipient of the A*STAR Research Attachment Programme in Singapore and Sheffield.

Sumei Sun (F'16) is currently the Head of the Communications and Networks Cluster, Institute for Infocomm Research, Agency for Science, Technology, and Research, Singapore, focusing on smart communications and networks for robust, QoS/QoE-guaranteed, and energy- and spectrum-efficient connectivity for human, machine, and things. She has authored or co-authored over 200 technical papers in prestigious IEEE journals and conferences, and holds 30 granted patents and over 30 pending patent applications, many of which have been licensed to industry. She was a recipient of the Top Associate Editor Award, in 2011, 2012, and 2015, all from the IEEE TRANSACTIONS ON VEHICULAR TECHNOLOGY. She was an Editor of the IEEE TRANSACTIONS ON VEHICULAR TECHNOLOGY, from 2011 to 2017, and the IEEE WIRELESS COMMUNICATION LETTERS, from 2011 to 2016. She has been serving as an Area Editor of the IEEE TRANSACTIONS ON VEHICULAR TECHNOLOGY, since 2017, and has been an Editor of the IEEE COMMUNICATIONS SURVEYS AND TUTORIALS, since 2015. She is a Distinguished Lecturer of the IEEE Vehicular Technology Society, from 2014 to 2018, a Distinguished Visiting Fellow of the Royal Academy of Engineering, U.K., in 2014, and has been the Vice Director of the IEEE Communications Society Asia–Pacific Board, since 2016. She has also been actively contributing to organizing IEEE conferences in different roles, including her recent services as an Executive Vice Chair of Globecom 2017, a Symposium Co-Chair of ICC 2015 and 2016, a Track Co-Chair of IEEE VTC 2016 Fall, and VTC 2017 Spring.

Xiaoli Chu (M'06–SM'15) received the B.Eng. degree in electronic and information engineering from Xi'an Jiao Tong University, in 2001 and the Ph.D. degree in electrical and electronic engineering from the Hong Kong University of Science and Technology, in 2005. She is a Reader with the Department of Electronic and Electrical Engineering, University of Sheffield, U.K. From 2005 to 2012, she was with the Centre for Telecommunications Research, King's College London. She has co-authored over 100 peer-reviewed journal and conference papers. She is a lead editor/author of the book entitled *Heterogeneous Cellular Networks—Theory, Simulation, and Deployment* (Cambridge University Press, 2013) and *4G Femtocells: Resource Allocation and Interference Management* (Springer, 2013). She was a co-recipient of the IEEE Communications Society 2017 Young Author Best Paper Award. She is an Editor of the IEEE COMMUNICATIONS LETTERS and the IEEE WIRELESS COMMUNICATIONS LETTERS. She was a Guest Editor of the IEEE TRANSACTIONS ON VEHICULAR TECHNOLOGY and the ACM/Springer *Journal of Mobile Networks and Applications*. She was the Co-Chair of Wireless Communications Symposium for the IEEE International Conference on Communications (ICC) 2015, a Workshop Co-Chair for the IEEE International Conference on Green Computing and Communications 2013, and has been a Technical Program Committee Co-Chair of six workshops on heterogeneous and small cell networks for IEEE ICC, GLOBECOM, WCNC, and PIMRC.

Tony Q. S. Quek (S'98–M'08–SM'12–F'17) received the B.E. and M.E. degrees in electrical and electronics engineering from the Tokyo Institute of Technology and the Ph.D. degree in electrical engineering and computer science from MIT. He is currently a Tenured Associate Professor with the Singapore University of Technology and Design (SUTD). He also serves as the Associate Head of ISTD Pillar and the Deputy Director of the SUTD-ZJU IDEA. His current research topics include wireless communications and networking, security, big data processing, network intelligence, and Internet-of-Things.

He has co-authored the book entitled *Small Cell Networks: Deployment, PHY Techniques, and Resource Allocation* (Cambridge University Press, 2013) and *Cloud Radio Access Networks: Principles, Technologies, and Applications* (Cambridge University Press, 2017). He has been actively involved in organizing and chairing sessions, and has served as a technical program committee member as well as symposium chair in a number of international conferences. He is currently an Elected Member of IEEE Signal Processing Society SPCOM Technical Committee. He was an Executive Editorial Committee Member of the IEEE TRANSACTIONS ON WIRELESS COMMUNICATIONS and an Editor of the IEEE TRANSACTIONS ON COMMUNICATIONS and the IEEE WIRELESS COMMUNICATIONS LETTERS.

Dr. Quek was a recipient of the 2008 Philip Yeo Prize for Outstanding Achievement in Research, the IEEE Globecom 2010 Best Paper Award, the 2012 IEEE William R. Bennett Prize, the 2015 SUTD Outstanding Education Awards—Excellence in Research, the 2016 IEEE Signal Processing Society Young Author Best Paper Award, the 2017 CTTC Early Achievement Award, the 2017 IEEE ComSoc AP Outstanding Paper Award, and the 2017 Clarivate Analytics Highly Cited Researcher.

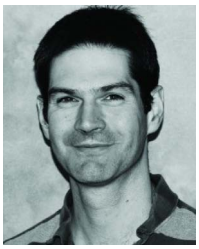

Alastair Buckley is a Senior Lecturer of organic electronics and photonics with the University of Sheffield. He moved to academia in 2008 following eight years in industrial research and development in polymer light emitting display device development and manufacturing with MicroEmissive Displays PLC. He has expanded his research to include organic PV devices and also interdisciplinary studies of the widespread integration of PV into society. This new research direction has resulted in improved understanding of the performance of U.K.-based PV systems and how PV integrates into the energy system. He leads U.K. web-based PV monitoring and forecasting services that have been developed to address the growing need of the U.K. energy sector to better manage its diversifying energy portfolio (https://www.solar.sheffield.ac.uk/pvlive/).